Submitted to ApJ September 1 2004

On the afterglow and host galaxy of GRB 021004: A comprehensive study with the *Hubble Space Telescope*[1]

J. P. U. Fynbo[2], J. Gorosabel[3,4], A. Smette[5,6], A. Fruchter[3], J. Hjorth[2], K. Pedersen[2], A. Levan[8], I. Burud[3], K. Sahu[3], P. M. Vreeswijk[5], E. Bergeron[3], C. Kouveliotou[12], N. Tanvir[9], S. E. Thorsett[11], R. A. M. J. Wijers[16], J. M. Castro Cerón[3,2], A. Castro-Tirado[4], P. Garnavich[13], S. T. Holland[14,15,16], P. Jakobsson[2], P. Møller[7], P. Nugent[10], E. Pian[17], J. Rhoads[3], B. Thomsen[18], D. Watson[2], and S. Woosley[11]

ABSTRACT

[2]NBI, Astronomical Observatory, University of Copenhagen, Juliane Maries Vej 30, DK–2100 Copenhagen Ø, Denmark

[3]Space Telescope Science Institute, 3700 San Martin Drive, Baltimore, MD 21218, USA

[4]Instituto de Astrofísica de Andalucía, IAA-CSIC, Granada, Spain

[5]European Southern Observatory, Casilla 19001, Santiago 19, Chile

[6]Research Associate, National Fund for Scientific Research (FNRS), Belgium

[7]European Southern Observatory, Karl Scwarzschild-Strasse 2, D-85748 Garching bei München, Germany

[8]Department of Physics and Astronomy, University of Leicester, University Road, Leicester, LE1 7RH, UK

[9]Department of Physical Science, University of Hertfordshire, College Lane, Hatfield, AL10 9AB, UK

[10]Lawrence Berkeley National Laboratory, 1 Cyclotron Road, Berkeley, CA 94720, USA

[11]Department of Astronomy and Astrophysics, University of California, 1156 High Street, Santa Cruz, CA 95064, USA

[12]NASA/Marshall Space Flight Center, National Space Science and Technology Center (NSSTC), SD-50, 320 Sparkman Drive, Huntsville, AL 35805, USA

[13]Astronomical Institute, University of Amsterdam, Kruislann 403, 1098 SJ Amsterdam, The Netherlands

[14]Department of Physics, University of Notre Dame, 225 Nieuwland Science Hall, Notre Dame, IN 46556, USA

[15]Swift Science Center, Goddard Space Flight Center, Code 660,1, Greenbelt, MD 20771-0003, USA

[16]Universities Space Research Association

[17]Osservatorio Astronomico di Trieste, Via G.B. Tiepolo 11, 34131 Trieste, Italy

[18]Department of Physics and Astronomy, University of Aarhus, Ny Munkegade, DK-8000 Aarhus C

We report on Hubble Space Telescope (*HST*) observations of the late-time afterglow and host galaxy of GRB 021004 ($z = 2.33$). Although this gamma-ray burst (GRB) is one of the best observed so far in terms of sampling in the time domain, multi-wavelength coverage and polarimetric observations, there is large disagreement between different measurements and interpretations of this burst in the literature. We have observed the field of GRB 021004 with the *HST* at multiple epochs from 3 days until almost 10 months after the burst. With STIS prism and G430L spectroscopy we cover the spectral region from about 2000 Å to 5700 Å corresponding to 600–1700 Å in the restframe. From the limit on the flux recovery bluewards of the Lyman-limit we constrain the H I column density to be above 1×10^{18} cm^{-2} (5σ). Based on ACS and NICMOS imaging we find that the afterglow evolved achromatically within the errors (any variation must be less then 5%) during the period of *HST* observations. The color changes observed by other authors during the first four days must be related to a 'noisy' phenomenon superimposed on an afterglow component with a constant spectral shape. This also means that the cooling break has remained on the blue side of the optical part of the spectrum for at least two weeks after the explosion. The optical–to–X-ray slope $\beta_{\rm OX}$ is consistent with being the same at 1.4 and 52.4 days after the burst. This indicates that the cooling frequency is constant and hence, according to fireball models, that the circumburst medium has a constant density profile. The late-time slope of the lightcurve (α_2, $F_\nu \propto t^{-\alpha_2}$) is in the range $\alpha_2 = 1.8$–1.9, although inconsistent with a single power-law. This could be due to a late-time flattening caused by the transition to non-relativistic expansion or due to excess emission (a 'bump' in the lightcurve) about 7 days after burst. The host galaxy is like most previously studied GRB hosts a (very) blue starburst galaxy with no evidence for dust and with strong Lyα emission. The star-formation rate of the host is about 10 M$_\odot$ yr^{-1} based on both the strength of the UV continuum and on the Lyα luminosity. The spectral energy distribution of the host implies an age in the range 30–100 Myr for the dominant stellar population. The afterglow was located very close (∼100 pc) to the center of the host implying that the progenitor was possibly associated with a circumnuclear starburst.

Subject headings: cosmology: observations — gamma rays: bursts —

---

[1]Based on observations made with the NASA/ESA *Hubble Space Telescope*, obtained at the Space Telescope Science Institute, which is operated by the Association of Universities for Research in Astronomy, Inc., under NASA contract NAS 5-26555. These observations are associated with programs 9074 and 9405.

1. Introduction

The very rapid localization of cosmic Gamma-Ray Bursts (GRBs) made possible with the HETE-2 satellite has enabled very well-sampled multi-band lightcurves ranging from a few minutes to several months after the bursts. One of the best studied GRBs so far is the bright burst detected on 2002 October 4 (all epochs are given as UT) with HETE-2 (Shirasaki et al. 2002). The optical afterglow was detected unusually early – 3.2 minutes after the high energy event (Fox et al. 2003) and monitored intensively from many telescopes in the following hours to months (e.g., Pandey et al. 2003; Holland et al. 2003 – hereafter H03; Bersier et al. 2003; Mirabal et al. 2003 – hereafter M03). The degree of polarization was measured on several epochs leading to the detection of a variable polarization angle (Rol et al. 2003). The redshift was determined to be $z = 2.33$ based on strong hydrogen and metal absorption lines as well as a Lyα emission line from the underlying host galaxy (Chornock & Filippenko 2002; Møller et al. 2002; Pandey et al. 2003; Matheson et al. 2003; M03). The absorption system associated with GRB 021004 contained several components covering a velocity range of more than 3000 km s^{-1} with clear evidence for line-locking between the components (Savaglio et al. 2002; Møller et al. 2002; Castro-Tirado et al. 2004).

Despite the intensive coverage of this afterglow there is quite limited agreement between the reported afterglow parameters and their interpretation, i.e., the spectral and late-time decay slopes, wind or ISM circumburst medium, and position of the cooling break (e.g., Lazzati et al. 2002; Pandey et al. 2003; Li & Chevalier 2003; Holland et al. 2003; Heyl & Perna 2003; Dado et al. 2003; Mirabal et al. 2003; Rol et al. 2003; Nakar et al. 2003; Björnsson, Gudmundsson & Jóhannesson 2004). The reasons are *i)* the very complex lightcurve during the first week and *ii)* the presence of a relatively bright host galaxy affecting the analysis of the late (fainter) part of the afterglow lightcurve.

In this paper we present an analysis of *HST* observations of the afterglow of GRB 021004 ranging from three days to ten months after the burst. Our emphasis is on the early UV spectroscopy, the late afterglow and on the properties of the host galaxy. In Sect. 2 we describe the observations, data reduction, and analysis and in Sect. 3 we present our discussion and conclusions. We assume $H_0 = 70$ km s^{-1} Mpc^{-1}, $\Omega_m = 0.3$ and $\Omega_\Lambda = 0.7$ throughout.

2. Observations and Data reduction

HST observed GRB 021004 after a fast turnaround on 2002 October 6–7. On 2002 October 6 we used the Space Telescope Imaging Spectrograph (STIS) to obtain near-UV spectroscopic observations of the afterglow. The Prism (4 orbits) as well as the G430L

grating (2 orbits) were used for the spectroscopic STIS observations. The observing log is given in Table 1. The choice of the Prism could appear surprising at first sight as it provides little coverage redwards of the Lyman edge at the GRB redshift. However, at the time of submitting the Phase II proposal, the redshift was expected to be $1.60 < z < 2.1$ based on the presence of a $z = 1.60$ Mg II system and the lack of strong Lyα absorption (Fox et al. 2002, Eracleous et al. 2002; Weidinger et al. 2002). The correct redshift $z = 2.33$ was only announced on 2002 October 8 (Chornock & Filippenko 2002) after the first *HST* observations. The reduction and analysis of the spectroscopic observations are described in Sect. 2.1.

Following the STIS observation the afterglow was observed with the Near Infrared Camera and Multi-Object Spectrometer (NICMOS) in the F110W and F160W filters and with the Advanced Camera for Surveys (ACS) High Resolution and Wide Field Cameras (HRC and WFC) in the four filters F250W, F435W, F606W, and F814W spanning nearly four octaves in wavelength from the near UV to the near-IR. The field was observed again on 2002 October 11, 2002 October 22, 2002 November 26, 2003 May 31, 2003 July 21, and 2003 July 26 in various WFC and NICMOS filters. The full journal of observations is listed in Table 1. The reduction and analysis of the NICMOS and ACS data are described in Sect. 2.2.

2.1. Spectroscopic STIS Observations

Reduction of the STIS observations were performed using the STIS Instrument Definition Team version of CALSTIS (Lindler 2003).

2.1.1. The Prism Spectra

The Prism dispersion is strongly wavelength dependent (for further details see the *HST* Instrument Handbook, Kim Quijano et al. 2003). The dispersion is 40 Å/pixel at 3000 Å, the expected wavelength of the Lyman edge at the GRB redshift and is smaller at longer wavelengths. Consequently, a Prism spectrum is quite sensitive to errors in the flat–field, especially for $\lambda > 3000$ Å. Also, the flux calibration is strongly dependent on the accuracy of the zero-point of the wavelength calibration. The overall calibration is unreliable for $\lambda > 3300$ Å. Over the 300 Å useful range of our spectra, these systematic effects were reduced by dithering the object along the slit between the four exposures.

In addition, the zero-point of the wavelength calibration also depends on the precise location of the object within the slit. Therefore, we compared the location of the afterglow

Table 1. The Log of *HST* STIS, ACS, and NIC3 Observations.

Date	Start (UT)	Filter	Exp.time (s)	Aper. (arcsec)	Countrate (counts s^{-1})	AB mag (total)	AB mag (OA)
STIS							
06/10/02	14:34:39	Prism	1300				
06/10/02	15:45:23	Prism	3×2625				
06/10/02	20:47:37	G430L	900+876				
06/10/02	22:09:39	G430L	1200+1261				
ACS							
07/10/02	04:42:16	F250W	2×2080	0.2	0.59±0.04	24.18±0.07	24.18±0.07
07/10/02	11:29:39	F435W	520	0.5	62.56±0.32	21.12±0.01	21.17±0.01
11/10/02	17:43:38	F435W	2×600	0.5	21.22±0.20	22.29±0.01	22.46±0.01
26/07/03	02:03:22	F435W	4×510	0.5	2.93±0.11	24.39±0.04	-
07/10/02	11:15:21	F606W	520	0.5	221.29±0.43	20.55±0.01	20.58±0.01
11/10/02	15:59:24	F606W	2×600	0.5	72.38±0.34	21.77±0.01	21.85±0.01
22/10/02	18:11:23	F606W	4×460	0.5/0.2	17.43±0.23	23.31±0.01	23.75±0.01
26/11/02	02:49:17	F606W	4×460	0.5/0.2	7.60±0.09	24.21±0.01	25.68±0.07
31/05/03	02:36:12	F606W	4×480	0.5	5.56±0.28	24.55±0.05	-
07/10/02	11:01:12	F814W	520	0.5	197.84±0.35	20.09±0.01	20.11±0.01
11/10/02	16:02:07	F814W	2×600	0.5	61.57±0.22	21.35±0.01	21.42±0.01
26/07/03	00:12:48	F814W	4×480	0.5	3.76±0.16	24.39±0.04	-
NIC3							
07/10/02	01:24:05	F110W	2×576	1.0	24.99±0.75	19.86±0.03	19.88±0.03
11/10/02	13:00:20	F110W	3×832	1.0	7.73±0.25	21.14±0.03	21.18±0.03
21/07/03	17:49:34	F110W	2×1280	0.5	0.29±0.03	24.62±0.10	-
07/10/02	03:09:20	F160W	576+512	0.5	31.90±0.96	19.41±0.03	19.43±0.03
11/10/02	14:18:05	F160W	3×832	1.0	9.90±0.30	20.68±0.03	20.74±0.03
22/10/02	16:46:47	F160W	3×832	1.0	2.25±0.15	22.29±0.08	22.57±0.09
25/11/02	07:34:57	F160W	3×832	0.5	0.76±0.10	23.38±0.13	24.67±0.50
26/05/03	00:54:09	F160W	2×1280	0.5	0.47±0.07	23.89±0.15	-

Note. — We here provide the photometry and the applied apertures sizes. The AB magnitudes are calculated from the countrates using synphot as described in Sect. 2.2.1. The effective central wavelengths of the filters are: 2714 Å (F250W), 4317 Å (F435W), 5918 Å (F606W), 8060 Å (F814W), 11229 Å (F110W), and 16034 Å (F160W).

Table 2: Countrate and Integrated Fluxes from the Prism Spectra

	Countrate photons/s	Flux	Flux (deconvolved)
	0.245±0.017	2.80±0.32	3.81±0.40
	0.231±0.011	2.42±0.19	2.37±0.21
	0.235±0.011	2.48±0.20	2.85±0.24
	0.251±0.011	2.64±0.21	3.31±0.27
Mean	0.240±0.006	2.59±0.12	3.08±0.14

Note. — The flux is given in units of 10^{-15} erg cm^{-2} s^{-1}.

in the acquisition image with the location of the slit center. The latter was measured by fitting a Gaussian at each row of an image of the slit on the CCD obtained with a Tungsten lamp obtained during the same visit. The centers of each fitted Gaussian were themselves fitted as a function of column number with a 3$^{\rm rd}$ degree polynomial. At the row where the afterglow image reaches a maximum intensity, the difference between the afterglow location and the slit center gives an offset of -0.064 pixels or $-0\farcs0016$, which we assume constant for each of the 4 spectra. The reduced spectrum is shown in Fig. 1. A break is seen in the spectrum at $\lambda \sim 3000$ Å.

The first two rows of Table 2 gives the countrate and the integrated flux over 3000 Å $< \lambda <$ 3300 Å, as well as their errors, for each Prism spectrum, and the last row gives the mean counts. These values are uncorrected for Milky Way extinction. There is no evidence that the afterglow flux varied during the course of these observations (about 5 hours). The absence of flux recovery shortward of the Lyman edge at $z = 2.323$ indicates a large H I column density. We return to this point in Sect. 2.1.3 below.

The spectra are also affected by the *HST* and STIS Point Spread Function: in particular, a significant fraction of the flux within 3000 Å $< \lambda <$ 3300 Å seen in Fig. 1 is actually spread out to apparently larger or smaller wavelength. Therefore we deconvolved the spectra using the method described in Smette et al. (2001). The integrated fluxes in the range 3000 Å $< \lambda <$ 3300 Å from the deconvolved spectrum along with the estimated errors are given in the last column of Table 2.

Table 3: Flux Densities Measured in the G430L Spectra

$\lambda_{\rm min}$ (Å)	$\lambda_{\rm max}$ (Å)	$\overline{\lambda}$ (Å)	Mean flux density
3305.00	3355.00	3329.58	3.35±0.43
3600.00	3650.00	3624.85	2.49±0.34
3840.00	3890.00	3864.04	2.70±0.36
4060.00	4110.00	4084.73	3.01±0.18
4370.00	4420.00	4394.04	2.97±0.15
4480.00	4530.00	4505.03	2.84±0.14
4690.00	4740.00	4714.40	2.91±0.14
4870.00	4920.00	4893.22	2.83±0.12
4990.00	5040.00	5018.06	2.98±0.12
5180.00	5230.00	5204.88	2.64±0.14
5350.00	5400.00	5373.63	2.72±0.12
5590.00	5640.00	5617.51	2.66±0.12

Note. — Flux densities given in 10^{-17} erg cm^{-2} s^{-1} Å^{-1}, corrected from Milky Way extinction.

2.1.2. The G430L Spectra

The G430L spectra cover the spectral range from 3000 Å to 5700 Å. The purpose of the observation was to determine the optical slope of the afterglow spectrum with good accuracy using near simultaneous observations over 3000–16000 Å together with the NICMOS data. As the GRB redshift was larger than foreseen when the Phase 2 was submitted, the spectra are affected by Lyα absorption and hence less useful for obtaining a precise measurement of the spectral slope. In addition, the spectra have a rather poor S/N and the telescope was not dithered between the 2 orbits as it was feared that the afterglow could be too faint for the processing of individual spectra. However, in order to limit the effect of the numerous cosmic rays, 2 CR–SPLIT exposures were made in each of the 2 orbits (cf. Table 1).

Due to the lack of dithering, correct processing of hot and warm pixels is crucial but in practice very difficult. The reduced individual spectra still show spikes. They are usually one or two pixel wide and often common between the different spectra. A number of criteria were defined to decide that a given pixel in the combined spectrum is not valid (i.e., due to

wrongly corrected warm or hot pixels) so that its value is not used in subsequent analysis: (a) its quality value is larger or equal to 175, which include among other conditions unrepairable hot pixels, pixels considered as cosmics by CR-SPLIT and saturated pixels, and hot pixels (CCD dark rate > 0.2 counts/s); (b) pixels with 'net' countrate larger than 0.09; and finally, (c) pixels with 'net' countrate smaller than -0.03 (blemishes). Figure 1 shows the resulting spectrum, its 1σ error spectrum, as well as boxes representing the mean values of valid pixels within a 50 Å range, and corresponding standard error. These wavelength ranges were selected away from the absorption lines reported by Matheson et al. (2003). Their limiting wavelengths as well as their corresponding mean fluxes and errors, corrected from Milky Way extinction, are reported in Table 3. The best fitted power-law over these ranges has a slope of $\beta = 1.71 \pm 0.14$ with a reduced $\chi^2 = 0.73$, significantly steeper than the $\beta \approx 1.0$ in the X-ray band (see below). In Sect. 2.2.3 we analyze the full Spectral Energy Distribution (SED) and conclude that the steep slope in the UV most likely is due to (modest) Small Magellanic Cloud (SMC) like extinction in the host galaxy. It is worth noting that the integrated flux of the deconvolved Prism spectrum over 3000 Å $< \lambda <$ 3300 Å, corrected for Milky Way extinction is $3.45 \pm 0.11 \times 10^{-15}$ erg cm^{-2} s^{-1}, while the corresponding value in the G430L spectrum is $3.15 \pm 0.46 \times 10^{-15}$ erg cm^{-2} s^{-1}. The fact that these two values are consistent with each other gives us confidence that the flux calibration of both spectra is correct.

2.1.3. Limit on the H I Column Density

Assuming that the underlying continuum can be represented by the extrapolation of the power-law described in the previous paragraph, we measure a total equivalent width of 1.9 ± 0.5 Å using the 6 pixels covering the range from 2417 to 2560 Å (redwards of the Lyman-limit of the foreground $z = 1.60$ Mg II absorber). The error is only the statistical error and it does not include the (likely larger) systematic error from the sky subtraction and flat-fielding. For a H I column density below 1×10^{18} cm^{-2} at $z = 2.33$, the continuum should have recovered, giving an equivalent width above 4.5 Å. Assuming no additional intervening strong (Lyman-limit) absorption, which is reasonable as there are no intervening metal line systems at $1.60 < z < 2.33$ (Møller et al. 2002), we conclude that the H I column density is larger than 1×10^{18} cm^{-2} (5σ). From the Lyα absorption line the column density is constrained to be below 1.1×10^{20} cm^{-2} (Møller et al. 2002). When we use the Voigt-profile parameters used to fit the low resolution spectrum presented in Møller et al. (2002) (a total column density of 6×10^{19} cm^{-2} and a b parameter of 15 km s^{-1}) we find that the predicted Lyβ lines appear weaker than the observed lines in the STIS spectrum. Therefore, either the total column density is larger than 6×10^{19} cm^{-2} or the b parameter is larger. Castro-Tirado

et al. (2004) find, based on a high resolution spectrum obtained with the UVES spectrograph on the VLT, that the absorption profiles all contain very wide components showing that the latter explanation appears to be the correct one. From the UVES spectrum the H I column density is constrained to be in the range 1–10$\times10^{19}$ cm^{-2}.

2.2. ACS and NICMOS Imaging Observations

The ACS observations from 2002 October 7 and 11 were CR-SPLIT observations consisting of only one or two exposures. These were reduced through the pipeline. The later epochs were observed with multiple exposures using non-integral multiple pixel dither steps and combined using MULTIDRIZZLE using pixfrac=1 and scale=0.66 (Fruchter & Hook 2002; Koekemoer 2002).

All NICMOS images were taken using the NIC3 camera (51×51 arcsec^2 field-of-view, 0.203 arcsec per pixel), MULTIACCUM mode (sample up the ramp), SPARS64 sample sequence and ∼3 arcsec dithers along each axis between exposures for bad pixel rejection. All data were taken in South Atlantic Anomaly free orbits except for the first two exposures of epoch 2. These were taken in an orbit following the last shallow pass of the day and were only mildly impacted, so correction for cosmic-ray persistence was not necessary. Two different calibration techniques were applied to this data. Epochs one, two and three (2002 October 7, 11 and 22, respectively) were calibrated with the standard NICMOS calibration pipeline CALNICA, using the best availbale reference files in the calibtration database. Following CALNICA, the STSDAS task PEDSKY was used to remove any remaining quad-based DC biases ("pedestal") signatures in the data. A sky image was constructed for each of the two filters using a source-masked median of all the epoch one and epoch two images combined, which were taken at different spacecraft orientations and dither positions. The sky image was then subtracted from each of the calibrated, PEDSKY corrected images.

For epochs four and five (2003 May 26 and July 21) a different technique was used, employing new methods developed during the Hubble Ultra Deep Field (HUDF) NICMOS analysis. First, a correction was made to the raw images to remove amplifier crosstalk from bright sources (also known as the "Mr. Stay-puft" anomaly). Although there are no bright sources in this field, every source produces a faint amplifier stripe and reflection to some level in the data. This is especially true of cosmic ray hits during the sample up the ramp MULTIACCUM exposures. Even though the cosmic ray hits themselves are flagged and rejected by the CALNICA processing, each hit leaves a faint stripe and reflection due to the amplifier effects, which can impact the noise floor. After this correction, the PEDSKY DC bias removal tool was run on dark-subtracted versions of each read up the ramp, and any

measured bias offset (per quadrant) and sky background was subtracted from the raw reads. An image of the sky background from the HUDF was used as the sky model in pedsky rather than the usual internal lamp flat. The entire MULTIACCUM sequence was then run through CALNICA as usual, except that the HUDF superdark was used instead of the standard dark reference file. This was possible because the same readout sample sequence that was used for the HUDF (SPARS64) was also used for these data.

2.2.1. Photometry

Photometry was done using aperture photometry. In Table 1 we provide measured countrates and the apertures sizes. For the 2002 October 7 and 11 observations the countrates in Table 1 are corrected for geometrical distortion using the Pixel Area Map from the STScI web-pages[19]. For the subsequent epochs this correction is done automatically during drizzling. To convert the measured countrates to magnitudes we used the *synphot* package under STSDAS. *Synphot* calculates the AB magnitude corresponding to the measured countrate and the applied aperture size. AB magnitudes derived in this way are given in the last column of Table 1.

To accurately measure the afterglow component in the 2002 October 22 and 2002 November 26 F606W observations, where the host galaxy is contributing a large fraction of the flux, we drizzled these images onto the coordinate system of the 2003 May 31 image. By subtracting the May 31 image we could then measure the afterglow component using a small aperture with radius 0.2 arcsec[20].

For the NICMOS images we use a circular aperture with radius equal to 5 pixels for the early points (October) and 2.5 pixels for the late points (November and later) due to the larger pixels of the NIC3 detector (the pixel scale is 0.203 arcsec per pixel). To derive AB magnitude we multiply the counts with 1.075 (early) and 1.15 (late) to compensate for the finite aperture and use the most recent photometric keywords available at the *HST* web-site[21] to get the zero-points.

---

[19] `http://www.stsci.edu/hst/acs/analysis/zeropoints/analysis/PAMS`

[20] We note that another transient source, presumably a supernova, is detected in the May 31 image superimposed on a faint galaxy at the celestial position RA(2000) = 00:26:55.8, Dec(2000) = 18:55:28.

[21] `http://www.stsci.edu/hst/nicmos/performance/photometry/nic13_postncs_keywords.html`

2.2.2. The Late-time Lightcurve

The ACS photometry allows a precise measurement of the late-time decay slope of the optical/near-IR afterglow lightcurve. There is a substantial disagreement between different reports in the literature. The values of the late-time decay slope ranges from $\alpha_2 = 1.43 \pm 0.03$ (H03 – note, however, that they argue for $\alpha_2 = 1.98$ as the best value when including also the broadband SED in the analysis) to $\alpha_2 = 2.9$ (M03). H03 find a jet-break time of 4.74 ± 0.14 days, M03 find 9 days (no error bar) and Björnsson et al. (2004) 0.6 days. The main reasons for these large disagreements are the very "bumpy" lightcurve (making the determination of the epoch of the jet-break very sensitive to the sampling of the lightcurve) and the relatively bright underlying host galaxy (potentially complicating the determination of the late time slope α_2). M03 assume an overly bright host galaxy magnitude (based on the November epoch of ACS observation in Table 1) and hence they derive an incorrectly large value of α_2. Rol et al. (2003) argue for a jet-break around 1 day based on the polarimetry, whereas Lazzati et al. (2004) find that a later jet-break time of about 3 ± 1 days is consistent with the polarimetry after day 1. Björnsson et al. (2004) are able to fit both the optical lightcurve, the radio and X-ray observations and the full evolution of the polarization using a model with four episodes of energy injection. In this model the real jet break takes place around 0.6 days and the apparent later break time is an artifact of the rebrightenings caused by energy injections.

The epoch 5 observation from May 31 2003 is more than half a year after the explosion, and the afterglow light at this epoch is most likely negligible. Conservatively assuming a late-time decay-slope of $\alpha_2 = 1.7$ we infer an afterglow magnitude of 28.5 in the F606W band at 2003 May 31. The decay-slope α_2 is larger than 1.7 (see below) and the afterglow magnitude at 2003 May 31 will therefore be fainter than 28.5. The rightmost column in Table 1 contains the afterglow magnitudes based on the assumption of no afterglow emission in the last epoch images. In Fig. 2 we plot the F606W magnitudes for epochs 1–4. Clearly, the four points are not consistent with a single power-law. Epoch 1 is before the break time as determined both by H03 and M03 and we can hence exclude this point from the power-law fit. However, a single power-law fit to the last three points is also formally rejected ($\alpha_2 = 1.86$, $\chi^2 = 9$, 1 d.o.f). The dotted line shows the result of an unweighted fit to the epoch 2–4 points, and the dashed line shows the line defined by the epoch 2 and 3 points. The dotted and dashed lines correspond to $\alpha_2 = 1.77$ and $\alpha_2 = 1.88$, respectively.

The last *HST* detection indicates a flattening of the late-time afterglow. This effect cannot be caused by residual afterglow emission in the epoch 5 image as this would have the opposite effect, making the lightcurve bend the other way. The flattening could be the result of the early transition to non-relativistic expansion. According to Livio & Waxman

(2000) α_2 should evolve towards $\sim$0.9 on a timescale of 5 months. An underlying supernova (Stanek et al. 2003; Hjorth et al. 2003a) is not expected to contribute significantly to the restframe UV light corresponding to the ACS filters. An alternative explanation is a bump in the light curve around 2002 October 11 causing the afterglow to be too bright. Given the very bumpy nature of the GRB 021004 lightcurve this does not appear unlikely.

2.2.3. The NIR/Optical SED of the Afterglow

The *HST* observations allow us to construct the SED of the afterglow around 2002 October $\sim$7.20 and $\sim$11.67. Given that the afterglow photometry is based on images where the host galaxy has been subtracted, the SED is not affected by host galaxy light contamination.

The *HST* photometry was shifted to a common epoch at 2002 October 7.20 and 11.67 assuming power-law decay slopes of $\alpha = 0.85$ (from H03) and $\alpha = 1.86$ (based on the analysis described above), respectively. The two observation sets are well clustered around these two common dates (maximum epoch shifts of $\delta t = 0.28$ days for October $\sim$7.20), so the derived SEDs are not very sensitive to the assumed values of α before the lightcurve break at $\sim$7.20 (e.g., $\delta m < 0.16$ for $0.5 < \alpha < 2.0$). We have added in quadrature a 0.05 mag error to the F110W-band magnitudes displayed in Table 1 in order to account for the NIC3 intra-pixel sensitivity variations. These sensitivity variations are especially relevant in the F110W-band and can produce sensitivity variations as large as 30% (peak-to-peak, Storrs et al. 1999).

We analyze the SED by fitting a function of the form $F_\nu \sim \nu^{-\beta} \times 10^{-0.4 A_\nu}$, where β is the spectral index and A_ν is the extinction at frequency ν. A_ν has been parametrized in terms of $A_{\rm V}$ following the three extinction laws Milky Way (MW), Large Magellanic Cloud (LMC), and SMC given by Pei et al. (1992). In the analysis we have included the UV flux from the STIS G430L spectrum (Table 3). The Pei et al. (1992) extinction laws are very uncertain for restframe wavelengths below 1000 Å, so the bluest bins of the STIS G430L spectrum were not included in the analysis. For the same reason, and also due to the Lyα blanketing and Lyman-limit absorption, the F250W data point was also not included in the SED fit. As a consistency check we have corrected the F250W data point for Lyα blanketing by convolving the F250W filter sensitivity curve with a Lyα blanketing model and a Lyman-limit break corresponding to the burst redshift. The two excluded data points are roughly compatible with the optical/NIR SED (the two stars in the upper panel of Fig. 3).

For both epochs the SEDs are clearly curved and hence highly inconsistent with a pure power-law spectrum (χ^2/d.o.f. $\geq$ 16.7, see Table 4). The LMC, and especially the MW extinction law which yields $A_{\rm V} < 0$, provide unacceptable fits. Only the SMC extinction

Table 4: Fits to the NIR/Optical SED

Extinction Law	Epoch UT 2002 Oct.	A_V	β	χ^2/d.o.f.
Unextincted	7.20	0	1.17 ± 0.02	18
MW	7.20	< 0	1.30 ± 0.03	19
LMC	7.20	0.32 ± 0.03	0.44 ± 0.06	12
SMC	7.20	0.23 ± 0.02	0.30 ± 0.06	3
Unextincted	11.67	0	1.15 ± 0.02	53
MW	11.67	< 0	1.26 ± 0.03	74
LMC	11.67	0.30 ± 0.03	0.47 ± 0.06	31
SMC	11.67	0.20 ± 0.02	0.42 ± 0.06	4

Note. — The table shows the SED fits for two epochs at October 7.20 and Oct 11.67. For each epoch the three extinction laws (MW, LMC and SMC) given by Pei et al. (1992) were considered. For completeness the unextincted pure power-law is also included. For both epochs, the best solution is clearly obtained with a SMC extinction law.

law provides moderate χ^2/d.o.f. values. The A_V and β values derived for the SMC ($\beta = 0.30 \pm 0.06$, $A_V = 0.23 \pm 0.02$ at October 7.20 and $\beta = 0.42 \pm 0.06$, $A_V = 0.20 \pm 0.02$ at October 11.67) are consistent with the ones reported by H03 at 2002 October 10.072: $\beta = 0.39 \pm 0.12$, $A_V = 0.26 \pm 0.04$.

The evolution of the afterglow is achromatic within the errors from 4000 Å to 16000 Å over the period from October 7 to October 22 (3 to 18 days after the burst). The F606W−F160W color from November 25–26 (53 days after the burst) observation is consistent with the color from the earlier epochs, but the error-bar is very large. H03 find that R−I is constant from 0.35 days to 5.5 days after the burst. On the other hand, Matheson et al. (2003) and Bersier et al. (2003) present evidence for color changes in the near-UV and optical range during the first four nights. The only way to reconcile these observations with ours is that the color changes must be related to a 'noisy' phenomenon superimposed on the normal afterglow light whose color remains very stable. In particular the cooling break cannot have passed through the optical range during the period from 0.35 to 18 days after the burst and possibly not earlier than 53 days.

2.2.4. Broadband SED

The X-ray afterglow of GRB 021004 was observed with the Chandra X-ray Observatory on 2002 October 5.9 and 2002 November 25 (Sako & Harrison 2002a,b) and is analyzed in H03 and Fox et al. (2003). The X-ray spectra show no evidence for absorption in addition to the foreground Galactic absorption with a 90% confidence upper limit on the absorbing column density in the host galaxy or along the line-of-sight of $2.3{\times}10^{21}$ cm^{-2}. H03 report a spectral slope in the X-rays of $\beta_X = 1.06 \pm 0.06$ and $\beta_X = 0.94 \pm 0.03$ fitting to 2–10 keV and 0.4–10 keV respectively. On November 25 (52.3 days after the burst) the X-ray flux was reduced to $7.2 \pm 2.5 \times 10^{-16}$ erg cm^{-2} s^{-1} compared to 4.3×10^{-13} erg cm^{-2} s^{-1} at around 1.5 days (Fox et al. 2003). This corresponds to a temporal decay slope in the X-rays of $\alpha_X = 1.80 \pm 0.10$ – very similar to what we find for the late-time slope in the optical/near-IR. This means that the broad-band SED from the optical to the X-ray band has a roughly constant shape $\sim$2 days and $\sim$52 days after the burst. In Sect. 3 we return to the interpretation of the broad-band SED within the context of the blast wave (fireball) and cannonball models.

In the lower panel of Fig. 3 the broadband SED from radio to X-rays is plotted. The epochs cluster around 2002 October 10.7, 11.67, and 2002 November 25.73. All the radio measurements and the X-ray flux of November 25.73 are taken from the literature. The X-ray points of October 7.20 (empty squares in the lower panel of Fig. 3) are based on our independent analysis of the Chandra X-ray spectrum taken on Oct 5.4–6.4 and shifted in time to October 7.20 assuming a decay of $\alpha = 1.86$ as derived from the optical light curve.

2.2.5. The Host Galaxy

The host galaxy is clearly detected in all bands in the latest epoch images from 2003 May–July. In the left panel of Fig. 4 we show a $1{\times}1$ arcsec^2 section of the F606W image from 2003 May 31 around the host galaxy. The host galaxy has a very compact core with a half light radius of only 0.12 arcsec. The resolution of the ACS image is about 0.05 arcsec so the core is well resolved. The galaxy has a faint second component offset by about 0.28 arcsec (2.2 kpc) towards the east. The position angle of the isophotes are twisting from a NE direction at the bright core towards an EW direction at the faintest levels.

The position of the afterglow is marked with a $\times$ and the 5σ error is shown with a circle ($1\sigma = 0.08$ pixels). The afterglow position is offset from the galaxy core by only 0.4 drizzled pixels, corresponding to 0.015 arcsec or 119 parsec at $z = 2.33$. This is one of the smallest impact parameters studied so far (Bloom, Kulkarni & Djorgovski 2002) implying that the

progenitor was possibly associated with a circumnuclear starburst.

The right panel of Fig. 4 shows a larger portion, 10×10 arcsec^2, of the field around the host galaxy. A a number of very faint (R > 26) galaxies are seen. Some of these are likely associated with the strong intervening Mg II absorbers at redshifts $z = 1.38$ and $z = 1.60$ seen in the afterglow spectrum (Møller et al. 2002; Castro-Tirado et al. 2004; see also Vreeswijk, Møller & Fynbo 2003; Jakobsson et al. 2004).

The SED of the galaxy can be quite well constrained from restframe 1200 Å to 5000 Å based on the ACS and NICMOS detections. This range brackets the UV region sensitive to young O and B stars, and hence the star formation rate, and the Balmer jump, sensitive to the age of the starburst. In Fig. 5 we show the SED of the host. The SED is essentially flat bluewards of the Balmer jump, and the Balmer jump has a magnitude of about 0.4 mag. Also shown is the simulated spectrum of a starburst from the 2003 version of the spectral synthesis models of Bruzual & Charlot (2003). The model starburst has an age of 42 Myr and a metallicity of 20% solar. It is possible to obtain reasonable fits with ages between 30 and 100 Myr dependent on the metallicity. In addition the range of allowed models could be increased by allowing for extinction, but as the galaxy is known to have high equivalent width Lyα line emission (Møller et al. 2002) there is little room for extinction (e.g., Charlot & Fall 1993). Based on the strength of the UV continuum of the host galaxy we can derive a value of the Lyα equivalent width (Møller et al. 2002 give a lower limit). The magnitude of the host galaxy of $\mathrm{F435W_{AB}} = 24.39 \pm 0.04$ corresponds to a specific flux of $F_\lambda = 1.1 \times 10^{-18}$ erg s^{-1} cm^{-2} Å^{-1}. With the measured line-flux of $F_{\mathrm{Ly}\alpha} = 2.5 \pm 0.5 \times 10^{-16}$ erg s^{-1} cm^{-2} we derive an observed equivalent width of 231 ± 47 Å corresponding to 69 ± 14 Å in the restframe, very similar to what is found for the host galaxy of GRB 000926 at $z = 2.04$ (Fynbo et al. 2002).

2.2.6. Star Formation Rate

The specific luminosity of the UV continuum provide a measurement of the star formation rate. We use the relation of Kennicutt (1998)

$$SFR(\mathrm{M_\odot\ yr^{-1}}) = 1.4 \times 10^{-28} L_\nu,$$

where L_ν is the specific luminosity in units (erg s^{-1} Hz^{-1}) in the 1500–2800 Å range. The observed AB magnitude of 24.45 corresponds to $F_\nu = 6.03 \times 10^{-30}$ erg s^{-1} Hz^{-1} cm^{-2}. In our choice of cosmology this corresponds to a value of $L_\nu = 4\pi d_l^2 F_\nu/(1+z) = 7.60 \times 10^{28}$ erg s^{-1} Hz^{-1}. This gives a SFR of 11 M$_\odot$ yr^{-1}. Due to dust absorption this is a lower

limit to the SFR, but as mentioned above there is only little room for dust. We can also derive an estimate for the SFR based on the Lyα flux. Møller et al. (2002) report a Lyα flux of $2.46\pm0.50\times10^{-16}$ erg s^{-1} cm^{-2}. This corresponds to a luminosity of $1.0\pm0.2\times10^{43}$ erg s^{-1} and a SFR of $10M_{\odot}$ yr^{-1} (following the calculation in Fynbo et al. 2002). The values of the SFR measured from the UV continuum and from the Lyα flux are hence in good agreement as for GRB 030323 (Vreeswijk et al. 2004). Hence, at least for some high-z starbursts Lyα emission is as reliable as the UV-continuum as SFR estimator (see Mas-Hesse et al. 2003 and Kunth et al. 2003 for critical discussions of the use of Lyα as SFR indicator).

3. Discussion and conclusions

3.1. The H I Column Density

The STIS spectroscopy is consistent with and complements what is known from ground based near-UV and optical spectroscopy. We detect the Lyman-limit break associated with the absorption system also detected in the Lyα resonance line and several metal lines at observer-frame optical wavelengths. Based on the Lyman-limit break we have placed a lower limit of about 1×10^{18} cm^{-2}, significantly higher than the $\sim 2\times10^{16}$ cm^{-2} inferred by M03 based on the Lyman series. The low column densities derived by M03 are caused by their assumption that the lines are not saturated. From the analysis of the X-ray afterglow Fox et al. (2003) derive an 90% confidence upper limit on the absorbing column density in the host galaxy or along the line-of-sight of 2.32×10^{21} cm^{-2}. The H I column density is quite low compared to that found for other GRB host galaxies (Vreeswijk et al. 2003, their Fig. 4 and discussion thereof). Most of the Lyα lines from GRB afterglows are strongly damped and have inferred column densities well above 10^{21} cm^{-2}. Only GRB 021004, GRB 011211 (Vreeswijk et al., in preparation) and possibly GRB 030226 (Klose et al. 2004) depart from this rule having column densities below the classical limit of 2×10^{20} cm^{-2} H I for Damped Lyα Absorbers in QSO spectra. The Lyα absorption profile is furthermore peculiar by having multiple components spread over about 3000 km s^{-1} with clear evidence for line-locking between the components (Savaglio et al. 2002; Møller et al. 2002; Castro-Tirado et al. 2004). The line-locking implies a very strong radiation field along the line of sight, presumably from the GRB progenitor star/star cluster, and it is possible that this radiation field has ionized the H I along the line thereby explaining the low total column density in the host galaxy. An alternative explanation for the low foreground column density compared to previously studied GRB lines-of-sight could be that the progenitor was located in the perimeter of the host galaxy.

3.2. Reddening

Despite the relatively low H I column density we detect statistically significant reddening in the afterglow SED. This is surprising if the dust properties of the ISM are similar to those of SMC dust like for previously studied GRB afterglows (e.g., Hjorth et al. 2003b). For the SMC extinction curve, for which $R_V = 2.93$ (Pei 1992), the observed extinction corresponds to E(B−V)=0.07. For a H I column density of 1–10$\times10^{19}$ cm^{-2} we derive a gas-to-dust ratio of N(H I)/E(B−V) = 1.5–15$\times10^{20}$ cm^2 mag^{-1}. This is significantly more reddening per column density than for SMC dust, where N(H I)/E(B−V) = 4.4$\pm$0.7$\times10^{22}$ cm^2 mag^{-1} (Bouchet et al. 1985). This could imply that a large fraction of the hydrogen along the line of sight is ionized. Alternatively, some of the reddening could be due to dust in the two foreground Mg II absorbers, but this appears unlikely as foreground absorbers in general cause very little reddening (Murphy & Liske 2004). In other words, the column densities of the foreground absorbers would have to have higher column densities than any known Damped Lyα Absorber, and this is very unlikely. The intrinsic shape of the afterglow SED is not expected to be a pure power-law as the cooling break is located very close to the near-UV/optical bands (see below). This may explain some of the difference, but we do not expect all the observed bending of the SED to be due to the intrinsic shape of the SED (see, e.g., Granot & Sari 2002).

3.3. Comparison with afterglow models

The post-break decay and spectral slope have been well constrained with the data presented in this paper. The spectral slope β in the optical to near-IR range corrected for extinction is 0.36 (mean value of the two measurements in Table 4). The late-time decay slope α_2 is in the range $\alpha_2 = 1.8$–1.9. These parameters agree well with the results found by H03. From these afterglow parameters we can infer the position of the cooling frequency ν_c relative to optical frequencies ν_O in the context of the standard blastwave model (see Mészáros 2002 for a review). For $\nu_c > \nu_O$ we expect $\alpha_2 - 2\beta = 1$, and for $\nu_c < \nu_O$ we expect $\alpha_2 - 2\beta = 0$ (Sari et al. 1999; Chevalier & Li 1999). Our observations imply $\alpha_2 - 2\beta = 1.0$–1.1, clearly indicating that $\nu_c > \nu_O$. This is consistent with the fact that the spectral slope in the X-rays, $\beta_X = 1.0$, is significantly larger than in the optical, which makes a spectral break between the optical and X-ray bands unavoidable. The change in slope of $\Delta\beta \approx 0.5$ is exactly what is expected across the cooling break, $\Delta\beta = 1/2$. We note that the strong bumps in the optical (and possibly X-ray lightcurves, Fox et al. 2003) can only be interpreted as being the result of density fluctuations if the cooling break is bluewards of the optical (and X-rays) (Lazzati et al. 2002, but see also Nakar et al. 2003; Nakar & Piran 2003; Björnsson et al.

2004). There is one complication with this conclusion: the number $N(E)$ as function of the electron energy $E = \gamma_e m_e c^2$ of the electrons producing the synchrotron emission is expected to have the form $N(E) \propto E^{-p}$, and for $\nu_c > \nu_O$ the theory predicts $\alpha_2 = p$. This means that $p \approx 1.9$, which results in a divergent energy spectrum. This case has been analyzed by Dai & Cheng (2001), but as p is in our case very close to 2 the resulting relations between decay and spectral slopes are quite similar to the equations for the $p > 2$ case.

The fact that the optical near-IR colors of the afterglow remains constant means that the cooling break has to be located on the blue side of the optical during the period from 0.35 days after the burst and at least until October 22 and possibly longer than November 25–26. Depending on the geometry of the blastwave and the density profile of the surrounding medium the cooling break will move towards higher frequencies (wind environment, Chevalier & Li 1999), lower frequencies (ISM, spherical geometry) or remain constant (ISM, jet geometry, Sari et al. 1999; Chevalier & Li 1999). The fact that the optical to X-ray slope β_{OX} has remained constant within the errors from October 7 and until November 26 with a value close to β_X means that the cooling frequency must have remained constant and close to the optical in this time span. This implies a jet geometry and a constant density environment. Li & Chevalier (2003) argue that an apparent break in the very early lightcurve ($t < 0.1$ days) is best understood assuming a wind-shaped circumburst medium. The only way to reconcile this with the discussion above is that the apparent break in the optical lightcurve is due to lightcurve fluctuations rather than being due to the typical frequency ν_m passing down from higher frequencies as suggested in the wind model of Li & Chevalier (1999).

The cannonball model offers an alternative explanation for the GRB phenomenon (Dado, Dar & De Rújula 2002). In this model the jet opening angle is much smaller, and the relativistic γ factor higher than in the fireball model. Dado, Dar & De Rújula (2003) have presented an analysis of GRB 021004 in the cannonball model in which a very good fit to most of the available groundbased data up to about 30 days after the burst was obtained. In the cannonball model the asymptotic (late-time) behavior of the afterglow is $F_\nu(t) \propto t^{-2.13}\nu^{-1.1}$ (Dado et al. 2002). The effective decay slope for the cannonball model fit GRB 021004 in Dado et al. (2003) between October 11 and November 25 is $\alpha_2 = 1.92$, which is close to the observed value. A spectral slope change towards $\beta = 1.1$ is not observed up to 50 days after the burst.

3.4. The Host Galaxy

The host galaxy is extremely blue in the observed optical bands. Fig. 6 shows the optical colors of the host in a color-color diagram. The points with error bars represent

galaxies in the environment of the host (from 70×70 arcsec^2 around the host) and the dots are colors of galaxies from the ACS observations of the GOODS South field[22]. As seen, the host is in the extreme blue color of the distribution for field galaxies. The reason for this is a combination of a young age (<100 Myr) and the redshift causing a very small Lyα blanketing in the F435W filter and placing the Balmer jump beyond the F814W band. The optical bands hence all probe the restframe UV continuum of the newly formed massive stars in the galaxy. A SFR of about 10 $M_\odot$ yr^{-1} is derived from the restframe UV flux density. The SFR derived from the Lyα luminosity is consistent with this value. The host galaxy has been observed in the sub-mm range with SCUBA (Tanvir et al. 2004), but it was not detected above a 2σ limit of 2.5 mJy. All evidence is consistent with the host being a young, dust-poor starburst. This is typically for GRB host galaxies (Fruchter et al. 1999; Le Floc'h et al. 2003; Christensen et al. 2004; Courty, Björnsson & Gudmundsson 2004).

So far, 10 GRBs have been detected at redshifts where Lyα is observable from the ground ($z \gtrsim 1.7$), namely GRBs 971214, 000131, 000301C, 000926, 011211, 020124, 021004, 030226, 030323, and 030429. Of these, the host galaxy of GRB 021004 is intrinsically the brightest. Nevertheless, it is fainter than the characteristic luminosity L^* for Lyman-break galaxies at slightly larger redshifts (e.g., Adelberger & Steidel 2000). The reason why most GRB host galaxies are relatively faint, dust-poor starbursts is not yet established. It could be that most of star-formation at these redshifts are located at the faint end of the luminosity function. There is evidence that the faint end slope of the luminosity function is significantly steeper than locally (Adelberger & Steidel 2000; Shapley et al. 2001), so this is not unlikely. However, there is still substantial uncertainty about the faint end slope (e.g., Gabasch et al. 2004). Another possibility is a low metallicity preference for GRBs as predicted by the collapsar model (MacFadyen & Woosley 1999; see also Fynbo et al. 2003; Le Floc'h et al. 2003, Prochaska et al. 2004). With the current very inhomogeneous sample of GRB host galaxies we cannot exclude that the current sample is strongly biased against dusty starbursts. The Swift mission offers the possibility to resolve this issue very soon (Gehrels et al. 2004).

We thank Arnon Dar and Gunnlaugur Björnsson for critical comments on earlier versions of the manuscript. Support for Proposal number GO 9405 was provided by NASA through a grant from the Space Telescope Science Institute, which is operated by the Association of Universities for Research in Astronomy, Incorporated, under NASA contract NAS5-26555. We thank the schedulers of the Space Telescope, and in particular our Program Coordinator, Ray Lucas, for the extraordinary effort they put in to assure timely observations. AJL ac-

[22]For the GOODS data we use the average of F775W and F850LP magnitudes as a proxy for F814W

knowledges support from the Space Telescope Science Institute Summer Student Programme and from PPARC, UK. STH acknowledges support from the NASA LTSA grant NAG5–9364. PJ acknowledges support from a special grant from the Icelandic Research Council. This work was conducted in part via collaboration within the the Research and Training Network "Gamma-Ray Bursts: An Enigma and a Tool", funded by the European Union under contract number HPRN-CT-2002-00294. This work was also supported by the Danish Natural Science Research Council (SNF) and by the Carlsberg Foundation.

REFERENCES

Adelberger, K. L., & Steidel, C. C. 2000, ApJ, 544, 218

Anupama, G. C., Sahu, D. K., Bhatt, B. C., & Prabhu, T. P. 2002, GRB Circular Network, 1582

Bersier, D. et al. 2003, ApJ, 584, L43

Björnsson, G., Gudmundsson, E., & Jóhannesson, G. 2004, ApJ, in press

Bloom, J. S., Kulkarni, S. R., & Djorgovski, S. G. 2002, AJ, 123, 1111

Bolzonella, M., Miralles, J.-M., & Pelló, R. 2000, A&A, 363, 476

Bouchet, P., Lequeux, J., Maurice, E., Prevot, L., & Prevot-Burnichon, M. L. 1985, A&A, 149, 330

Bruzual, G., & Charlot, C. 2003, MNRAS, 344, 1000

Castro-Tirado, A. J., et al. 2004, Science, submitted

Charlot, S., & Fall, S. M. 1993, ApJ, 405, 538

Chevalier, R. A., & Li, Z.-Y. 1999, ApJ, 520, L29

Chornock, R., & Filippenko, A. V. 2002, GRB Circular Network, 1605

Christensen, L., Hjorth, J., & Gorosabel, J. 2004, A&A, in press (astro-ph/0407066)

Courty, S., Björnsson, G., & Gudmundsson, E. H. 2004, MNRAS, in press (astro-ph/0407359)

Dado, S., Dar, A., & De Rújula A. 2002, A&A, 388, 1079

Dado, S., Dar, A., & De Rújula A. 2003, ApJ, 585, L15

Eracleous, M., Schaefer, B. E., Mader, J., & Wheeler, C. 2002, GRB Circular Network, 1579

Fox, D.W. et al. 2002, GRB Circular Network, 1569

Fox, D. W., et al. 2003, Nature, 422, 284

Fruchter, A. S., et al. 1999, ApJ, 519, L13

Fruchter, A. S., & Hook, R. 2002, PASP, 114, 144

Fynbo, J. P. U., et al. 2002, A&A, 388, 425

Fynbo, J. P. U., et al. 2003, A&A, 406, L63

Gabasch, A., et al. 2004, A&A, 421, 41

Gehrels, N., et al. 2004, ApJ, 611, 1005

Granot, J., & Sari, R. 2002, ApJ, 568, 820

Heyl, J. S., & Perna, R. 2003, ApJ, 586, L13

Hjorth, J., et al. 2003a, Nature, 423, 847

Hjorth, J., et al. 2003b, ApJ, 597, 699

Holland, S. T., et al. 2003, AJ, 125, 2291 (H03)

Jakobsson, P., et al. 2004, A&A, in press (astro-ph/0407439)

Kennicutt, R. C. 1998, ARA&A, 36, 189

Kim Quijano, J., et al. 2003, STIS Instrument Handbook, version 7.0, (Baltimore: STSCI)

Klose, S., et al. 2004, AJ, in press (astro-ph/0408041)

Koekemoer, A. M. et al. 2002, "HST Dither Handbook", Version 2.0 (Baltimore: STScI)

Kunth, D., Leitherer, C., Mas-Hesse, J. M., Östlin, G., & Petrosian, A. 2003, ApJ, 597, 263

Lazzati, D., Rossi, E., Covino, S., Ghisellini, G., & Malesani, D. 2002, A&A, 396, L5

Lazzati, D., et al. 2003, A&A, 410, 823

Le Floc'h, E., et al. 2003, A&A, 400, 499

Li, Z.-Y., & Chevalier, R. A. 2003, ApJ, 589, L69

Lindler, D. J. 2003, CALSTIS Reference Guide http://hires.gsfc.nasa.gov/stis/docs/calstis/calstis.html

Livio, M., & Waxman, E. 2000, ApJ, 538, 187

Mas-Hesse, J. M., et al. 2003, ApJ, 598, 858

Matheson, T., et al. 2003, ApJ, 582, L5

Mészáros, P. 2002, ARA&A, 40, 137

Mirabal, N., et al. 2003, ApJ, 595, 935 (M03)

Møller, P., Warren, S. J., Fall, S. M., Fynbo, J. P. U., & Jakobsen, P. 2002, ApJ, 574, 51

Møller, P., et al. 2002, A&A, 396, L21

Murphy, M. T., & Liske, J. 2004, MNRAS, submitted (astro-ph/0405472)

Nakar, E., Piran, T., & Granot, J. 2003, NewA, 8, 495

Nakar, E., & Piran, T. 2003, ApJ, 598, 400

Pandey, S. B. et al. 2003, Bull. Astron. Soc. India, 31, 19

Prochaska, J. X., et al. 2004, ApJ, 611, 200

Rol, E., et al. 2003, A&A, 405, L23

Sahu, D. K., Bhatt, B. C., Anupama, G. C., & Prabhu, T. P. 2002, GRB Circular Network, 1587

Sako, M., & Harrison, F. 2002a, GRB Circular Network, 1624

Sako, M., & Harrison, F. 2002b, GRB Circular Network, 1716

Sari, R., Piran, T., & Halpern, J. P. 1999, ApJ, 519, L17

Savaglio, S. 2002, GRB Circular Network, 1633

Shapley, A. E., et al. 2001, ApJ, 562, 95

Shirasaki, Y., et al. 2002, GRB Circular Network, 1565

Smette, A., et al. 2001, ApJ, 556, 70

Stanek, K. Z., et al. 2003, ApJ, 591, L17

Storrs, A., Hook, R., Stiavelli, M., Hanley, C., & Freudling, W. 1999, STScI Instrument Science Report NICMOS-99-005

Tanvir, N. R., et al. 2004, MNRAS, 352, 1073

Vreeswijk, P. M., Møller, P., & Fynbo, J. P. U. 2003, A&A, 409, L5

Vreeswijk, P., et al. 2004, A&A, 419, 927

Weidinger, M., et al. 2002, GRB Circular Network, 1573

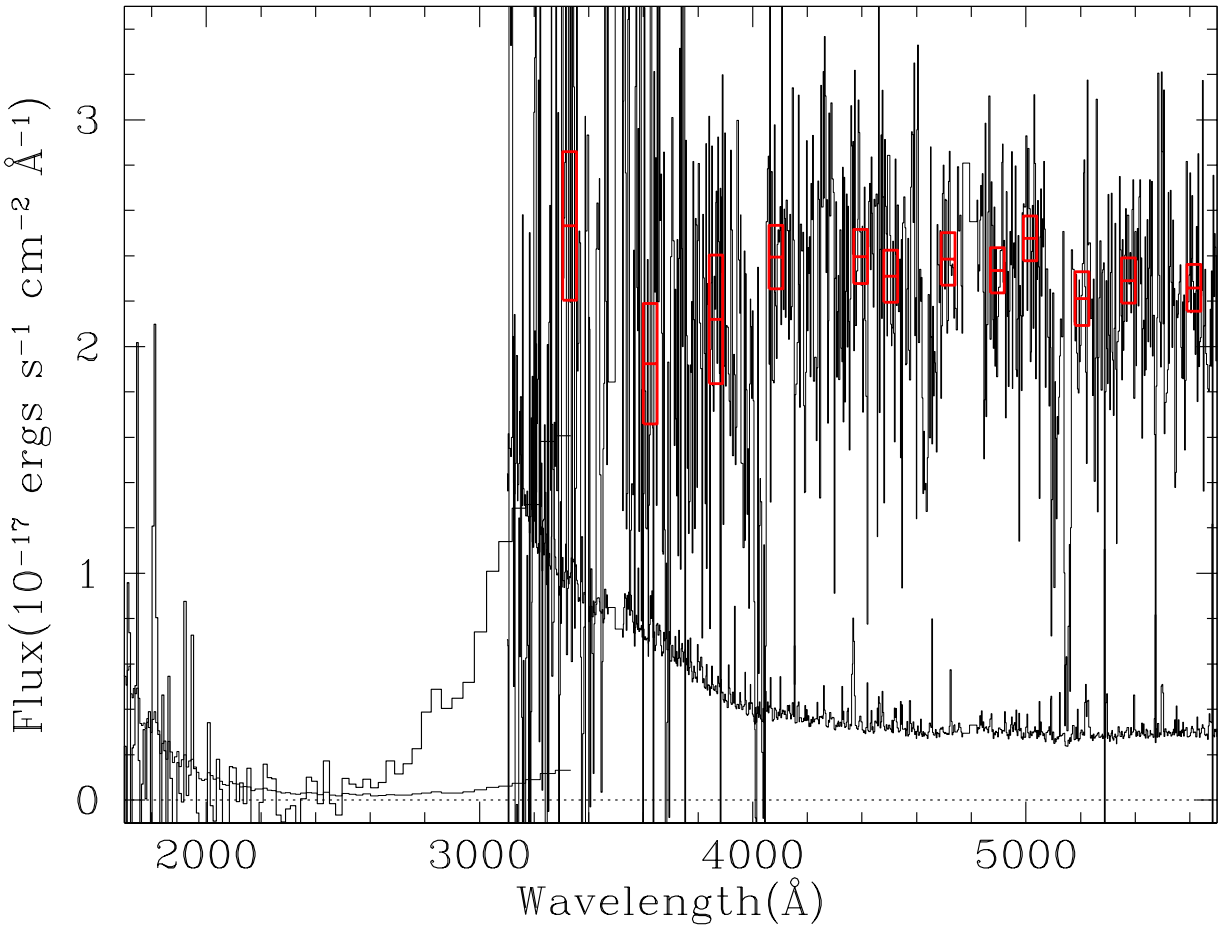

Fig. 1.—
HST STIS spectra of GRB 021004 taken on 2002 October 6. The Prism spectrum is the histogram extending from below 2000 Å to about 3300 Å. The G430L spectrum extends from about 3000 Å to 5500 Å. The sharp drop in flux around 3000 Å is the Lyman-limit absorption edge due to neutral hydrogen in the host galaxy. The red boxes show the average flux densities in wavelength ranges free of strong Lyα forest lines. For both the G430L and Prism spectra the 1σ spectra are also shown.

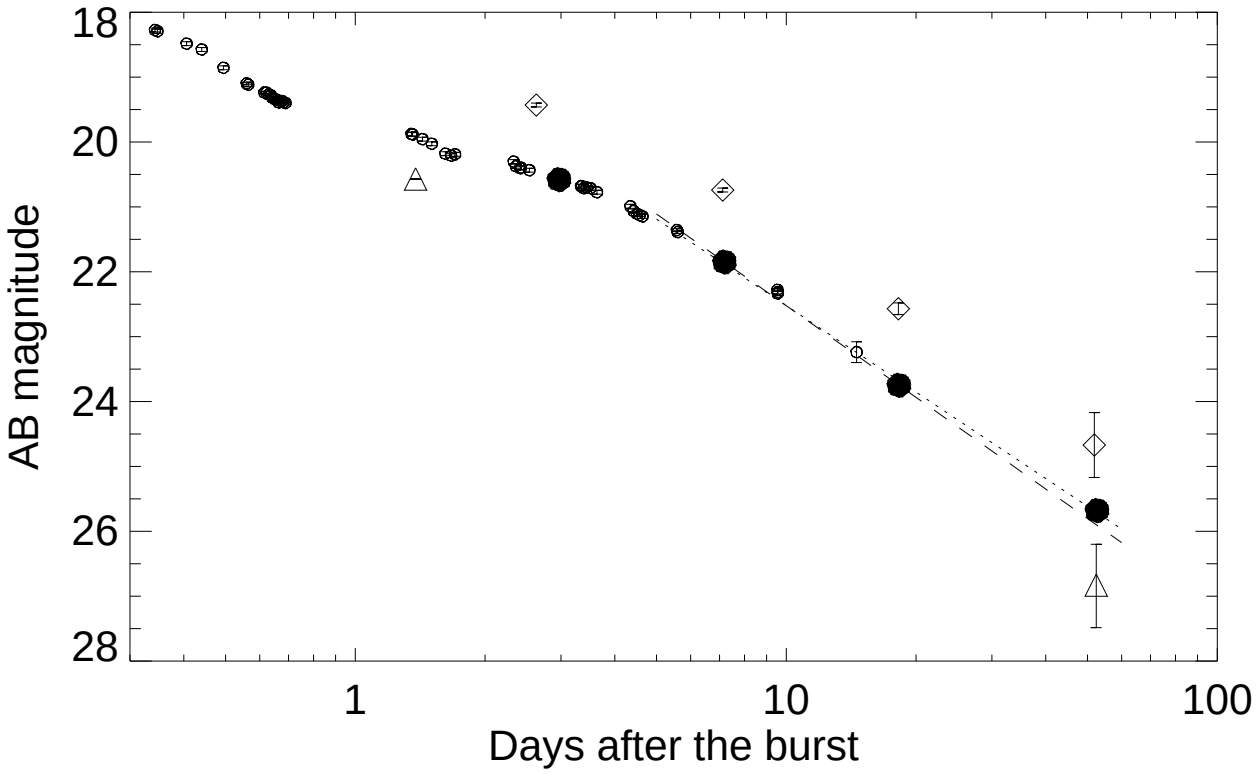

Fig. 2.—
The lightcurve from 0.3 days to 53 days after the GRB. The HST point are shown with filled circles (error bars smaller than the symbol sizes). The small, open circles are the ground based R-band data from H03 shifted to F606W AB magnitudes by adding 0.25 mag and corrected for a host magnitude of R(AB) = 24.40. The lightcurve seems to be flattening at late times, which could be due to the transition to non-relativistic expansion, but also due to bumps in the lightcurve around 2002 October 11. We also plot the four F160W points and the two X-ray points (arbitrarily shifted in flux) as diamonds and triangles with error-bars. These points indicate an achromatic evolution of the afterglow from the H-band to the X-ray band over a period of up to 50 days after the GRB.

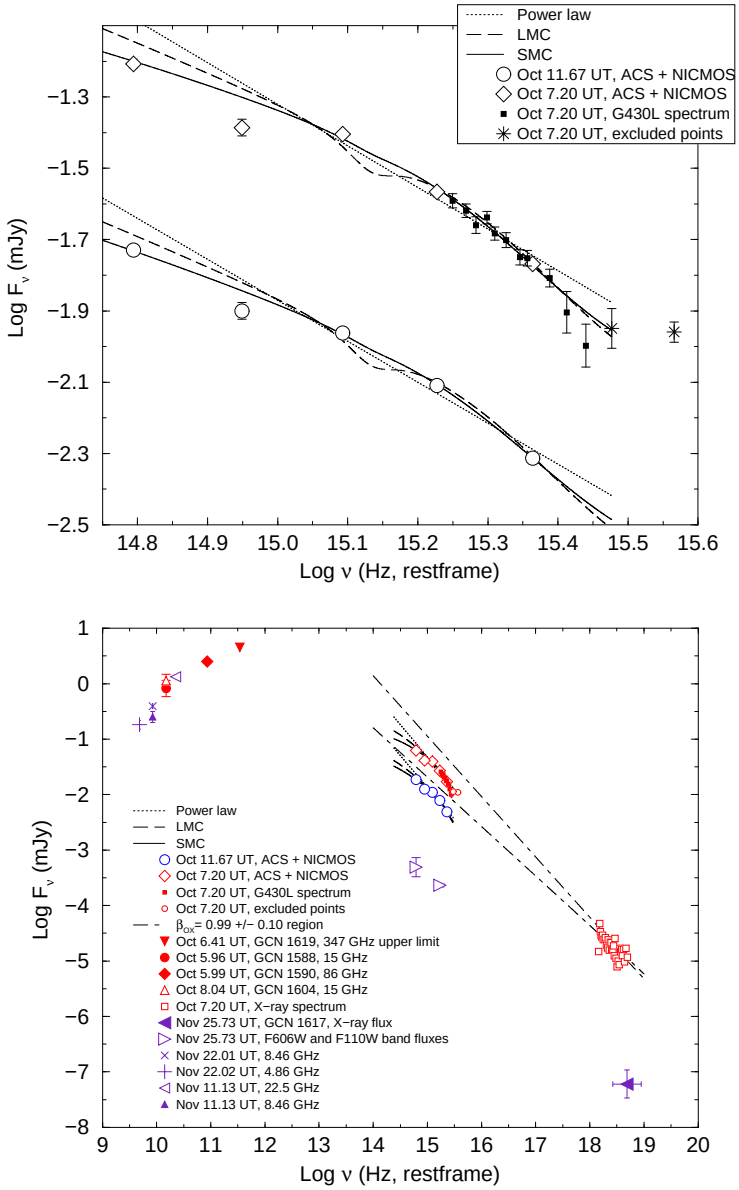

Fig. 3.—
Upper panel: The SED of the afterglow on 2002 October 7.2 (rhomboids) and 2002 October 11.67 (circles).The fluxes derived from the bins of the STIS G430L spectrum (see Table 3) have been shifted to 2002 October 7.2 and are shown with filled squares. The stars show the two data points (the F250W and the bluest bin of the STIS G430L spectrum) with a restframe wavelength below 1000 Å. These are not been included in the fits. The fit obtained with a MW-like extinction law is not displayed since it provides unphysical negative $A_{\rm V}$ values (see Table 4). *Lower panel*: The broadband SED of the GRB 021004 afterglow, from radio to X-rays. The plot represents the SED at Oct 2002 7.2, 11.67 and 2002 November 25.73. As shown, the broad band SED from the optical to the X-ray range has roughly a constant spectral index ($\beta_{\rm OX} \approx 1$). The dot-dashed line represents the 1σ region of the extrapolated $\beta_{\rm OX} = 0.99 \pm 0.1$ power-law fit derived by H03.

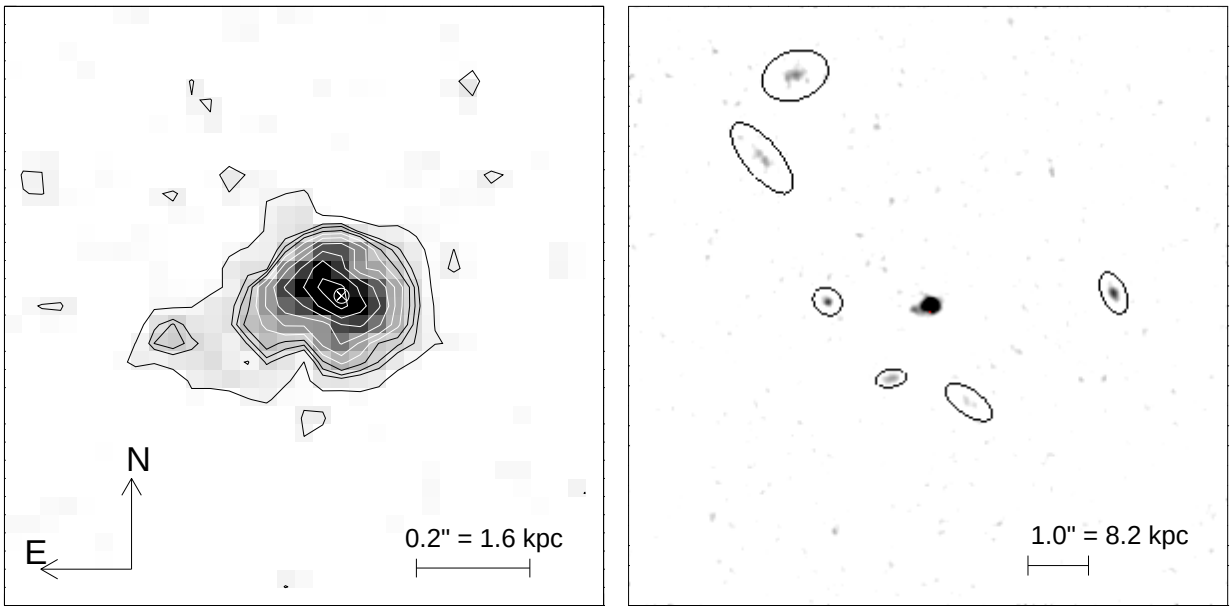

Fig. 4.—
Left panel: A 1×1 arcsec^2 section of the ACS/F606W image from 2003 May 31 around the host galaxy of GRB 021004. The GRB went off near the center of the galaxy (position marked with a cross and an error circle). To better show the morphology of the object we have overplotted contours with a logarithmic scaling. *Right panel:* A smoothed version of the ACS/F606W image from 003 May 31 covering 10×10 arcsec^2 centered on the host galaxy. As seen, there are a six very faint ($\gtrsim$ 26 mag, marked with ellipses) galaxies within 5 arcsec from the line-of-sight to the host galaxy. Some of these galaxies could be associated with the two Mg II absorbers detected in the afterglow spectrum.

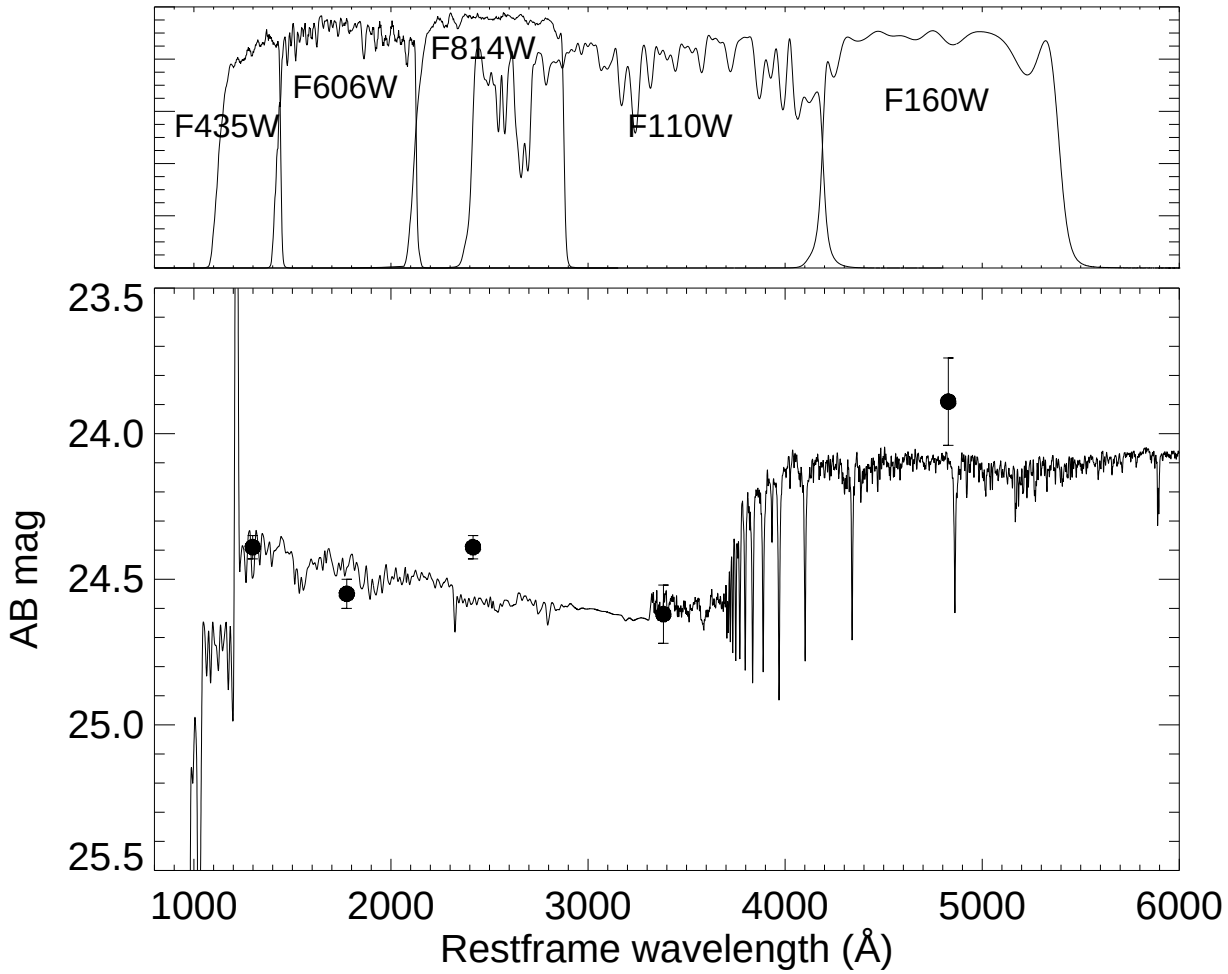

Fig. 5.—
The SED of the host galaxy extending from about 1200 Å to 5000 Å in the restframe. Also shown is the spectral synthesis model of a 42 Myr old star burst with $Z = 0.004$ and with a Lyα emission line added in by hand. The top panel shows the filter transmission curves corresponding to the five photometric points.

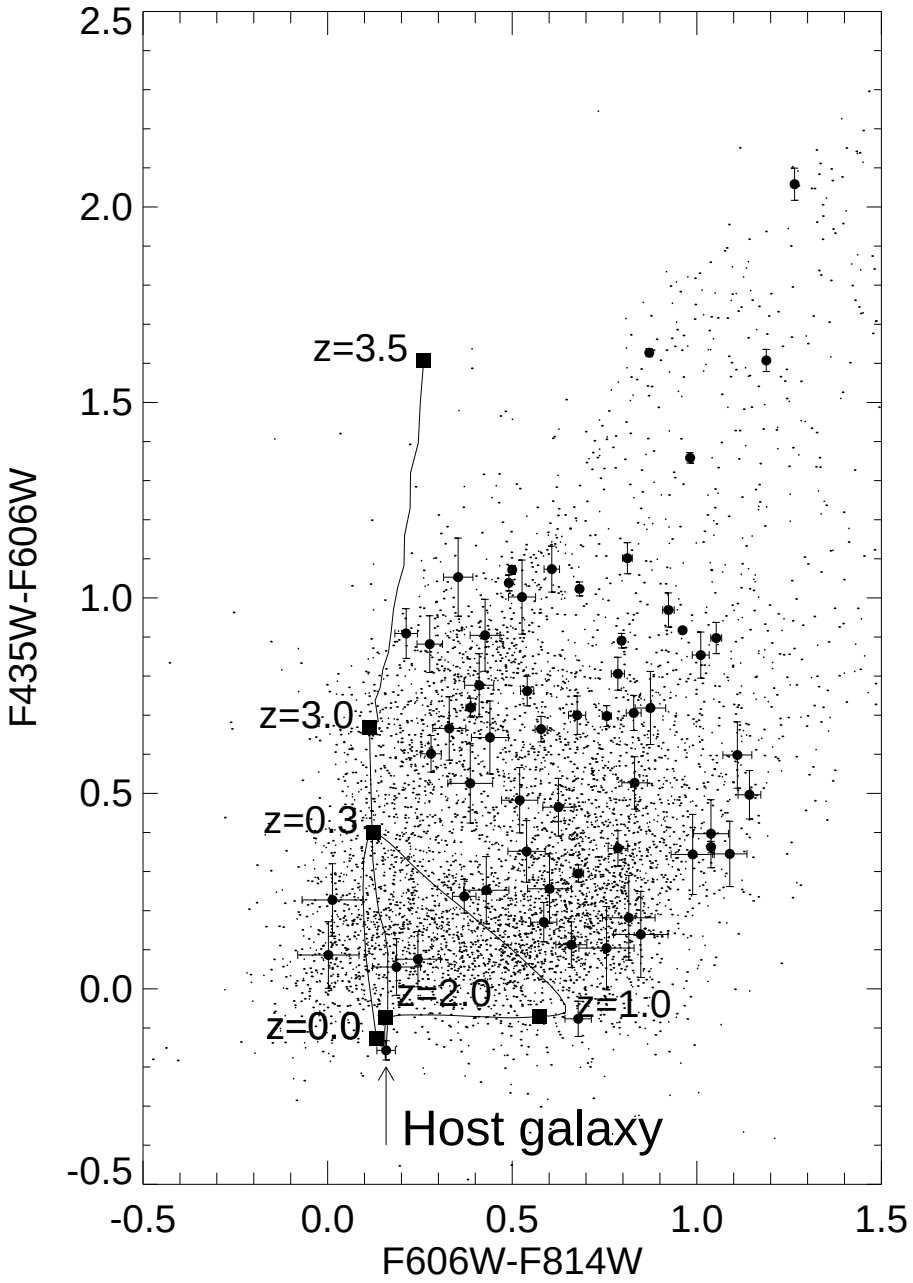

Fig. 6.—
The color of the host compared to the colors of galaxies in its environment (filled circles with error bars) and to galaxies in the GOODS South field (dots). Also shown are the colors of the spectral synthesis model shown in Fig. 5 as a function of redshift from $z = 0$ to $z = 3.5$ renormalized to go through the host galaxy point.